Proceedings of the 21st ICSMGE, Vienna, Austria, 14 – 19 June 2026. Pistrol, Adam & Schweiger (eds.)
Published by: ÖGG, Austrian Society for Geomechanics, Salzburg, Austria, ISBN 978-3-9503898-4-5
https://doi.org/10.53243/ICSMGE2026-452

The influence of oedometer sample aspect ratio on the observed compression behaviour of sand under different initial states

Ruan A. Murison*, Yashay Narainsamy, Gerhard Heymann, SW Jacobsz
*Department of Civil Engineering, University of Pretoria, South Africa, *ruan.murison@tuks.co.za*

Tiago A.V. Gaspar
Department of Civil and Environmental Engineering, Imperial College London, United Kingdom

ABSTRACT: Understanding the compression behaviour of a soil has important applications in predicting both volume change and shear response of a soil element in situ. It is generally accepted that remoulded clay-like soils have a unique normal consolidation line. Conversely, coarse-grained soils are likely to have multiple normal consolidation lines, meaning that investigations at various initial densities may be required. For dense granular soils, side wall friction may induce errors in the one-dimensional compression behaviour measured in the oedometer. Six oedometer tests were conducted on a remoulded silica sand. Initially loose samples and initially medium dense samples were tested in oedometer rings with height-to-diameter ratios ranging from 0.254 to 0.400. The initially loose samples exhibited no significant influence of sample aspect ratio on the measured normal consolidation line and swelling lines. The medium dense samples showed greater compressibility with increasing sample diameter. The normal consolidation line measured for the medium dense sample with the highest aspect ratio was approximately parallel to the normal consolidation lines of the initially loose samples. The undermeasurement of compressibility for dense granular soils when the sample aspect ratio is not sufficiently minimised was attributed to dilation at the soil–ring interface.

KEYWORDS: Compression behaviour; oedometer testing; side wall friction; dilation.

1 INTRODUCTION

Understanding the compression behaviour of a particular soil is important for many geotechnical applications, the most obvious being the prediction of volume changes, such as settlement of an embankment or building foundation. However, the principles of critical state soil mechanics imply that the compression and shear behaviour of soils are fundamentally linked. The response of a soil in drained or undrained shear depends on both its volumetric state (i.e. void ratio) and stress state. For this reason, understanding the compression behaviour of a particular soil may be key to understanding the strengths that can be mobilised and the stress paths followed when the soil is subjected to shearing. Investigations of the compression behaviour of granular soils are of particular interest to tailings dams (where consolidation occurs under self-weight and through desiccation) and compacted earth embankment dams (where consolidation and unloading occurs due to mechanical compaction), both for predictions of volume change and response during shearing. It is accepted that many coarse-grained materials, such as clean sands, do not have one unique normal consolidation line. For this reason, it is of particular importance for the engineer to thoroughly characterise the compression behaviour and understand the compression framework applicable to the soil, to know whether a soil element subjected to a certain stress path in the field would exist in a wet-of-critical ('contractive') or dry-of-critical ('dilative') state. Oedometer testing is an attractive option for characterisation of compression behaviour, due to the relative simplicity of the test and the wide stress range that may be investigated. However, for coarse-grained soils with high friction angles, side wall friction on the soil–ring interface in the oedometer may cause errors in the measured compression behaviour. This study aims to investigate the influence of the aspect ratio of an oedometer sample on the compressibility of a cohesionless silica sand under different initial relative densities.

2 COMPRESSION FRAMEWORK FOR SANDS

Terzaghi's theory of one-dimensional consolidation (Terzaghi, 1923; 1925) was likely the earliest theory on the compression of soils and is still widely implemented in practice a century later. The theory was founded on eight key assumptions, one of which was that a unique relationship between void ratio and effective stress exists for a given normally consolidated soil. However, the appropriateness of this assumption depends on soil type. It is widely accepted that the normal consolidation line (NCL) for a remoulded plastic clay is indeed unique. Experimental evidence of this assumption after Rendulic (1937), Skempton (1944), and Henkel (1960) was the basis of the proposition of the Rendulic or Roscoe surface in critical state soil mechanics (e.g. Schofield & Wroth, 1968; Roscoe & Burland, 1968). This is a unique state boundary surface in void ratio vs mean effective stress vs deviatoric stress space upon which wet-of-critical remoulded clays yield. The unique intrinsic normal consolidation line (ICL) for a reconstituted clay forms the basis of a framework proposed by Burland (1990), where any state plotting beyond the ICL may only be attained due to soil structure (Leroueil & Vaughan, 1990).

For non-plastic clean sands, the existence of a unique NCL or ICL is not realistic. Ishihara et al. (1975) proposed that an infinite number of normally consolidated states may exist for a sand. Further investigation by Jefferies & Been (2000) on a uniformly graded clean sand, prepared over a range of initial void ratios without imposing any stress history, led to the proposition of an infinite number of normal consolidation lines which are approximately parallel at low to moderate stresses. They also found that if a sample is unloaded and reloaded from any of these NCLs, it should follow along one of infinitely many elastic "swelling lines" at a flatter slope, as is the case for a clay with a unique NCL. The binding curve for permissible states within which a sand can exist (i.e. the state boundary surface) is known as the limiting compression curve (LCC). The mechanism causing compression paths of sands to converge onto this boundary at high stresses is particle crushing (fragmentation and breakage), as proposed by Pestana & Whittle (1995). The different idealised compression frameworks for clays and sands are illustrated in Figure 1. For non-textbook soils other than clean sands or plastic clays (e.g. natural silts, organic soils, mine tailings), the presence of a unique NCL may need to be investigated, as was done in a study on gold tailings by Narainsamy et al. (2023).

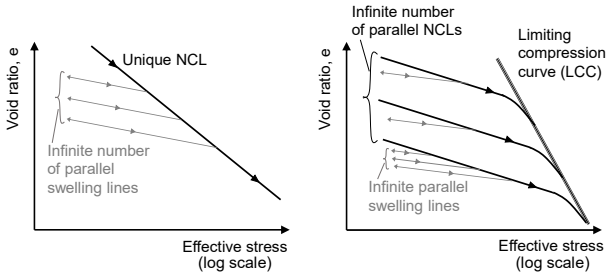

a) Clays b) Sands

Figure 1. Compression frameworks compatible with critical state soil mechanics.

3 BOUNDARY CONDITIONS IN OEDOMETER TESTING

The oedometer test is a popular test for determining one-dimensional consolidation properties of soils. One-dimensional deformation occurs under K_0 conditions (zero lateral strain) through the provision of a sufficiently stiff ring to restrain radial deformation. To ensure no variation of the applied stress with depth within the soil element being tested, a frictionless soil-ring interface is required. In practice however, shear stresses due to side wall friction may be mobilised along the interface. A simplified free body diagram of the stresses acting upon a soil element at the end of a consolidation increment (i.e. after the dissipation of all excess pore pressures) in a conventional fixed-ring oedometer test is provided in Figure 2a. In the figure, it was assumed that the self-weight of the soil sample is negligible, and that the magnitude of hydrostatic porewater pressure is small enough to be disregarded. It is recognised that the shear stress mobilised along the side wall would vary with depth, but the average shear stress over the entire height of the wall has been represented as τ_{avg}. To maintain equilibrium at any given depth within the sample, both the vertical effective stress (σ'_{v}) and resulting horizontal effective stress (σ'_{h}) would vary with depth as well. The stresses acting upon the element may be resolved into the resultant forces depicted in Figure 2b. The resultant force acting radially on the soil-ring interface is inclined at the interface friction angle (δ). The maximum variation in vertical effective stress experienced due to friction losses occurs between the applied stress at the top of the sample and the resultant normal stress at the bottom of the sample (σ'_{b}). If each of the terms in the expression for the resultant force at the bottom of the sample ($\mathrm{F_b}$) in Figure 2b is divided by the sample area, it can be shown that the maximum variation in vertical effective stress (assuming zero self-weight and pore pressure) is given by:

$$\sigma'_{\mathrm{v}} - \sigma'_{\mathrm{b}} = 4\tau_{avg} \cdot \frac{H}{D} \qquad (1)$$

Although it only holds true for this simplified case, Equation 1 shows that two options are available for limiting the errors that arise due to shear stresses at the soil-ring interface:

- reduce the roughness of the oedometer ring to reduce the interface friction angle, and thus reduce the mobilised shear stress on the interface (τ_{avg});
- reduce the height-to-diameter aspect ratio (H/D) of the oedometer ring, to reduce the influence of the shear stress that is mobilised.

Oedometer rings are usually made from stainless steel or brass with a polished surface to reduce side wall friction. ASTM D2435 (2020) recommends an aspect ratio of $H/D < 0.4$ such that the effects of side wall friction may be ignored.

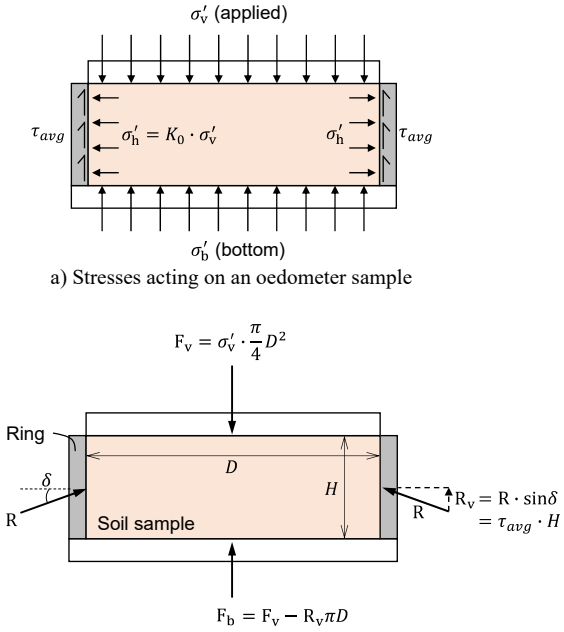

a) Stresses acting on an oedometer sample

b) Resultant forces acting on the sample

Figure 2. Simplified free body diagram of a fixed-ring oedometer sample at the end of a consolidation increment, assuming that sample self-weight and static porewater pressure are negligible.

4 EXPERIMENTAL WORK

4.1 *Material classification*

The material used in this study was a fine uncemented silica sand called *Cullinan Sand*, obtained from quarried sandstone and used for physical modelling at the University of Pretoria. The soil classifies as a uniformly graded slightly silty sand according to the Unified Soil Classification System (USCS) per ASTM D2487 (2017). The specific gravity of the sand was determined using a gas pycnometer per ASTM D5550 (2014). The particle size distribution (PSD) was determined using the laser diffraction technique per ISO 13320 (2020) and is given in Figure 3. The minimum dry density was determined by averaging values obtained according to Methods A and C in ASTM D4254 (2016) for an oven dry state, and the maximum dry density was determined per Method 1A in ASTM D4253 (2016), with the test also conducted on oven-dried sand. Properties of the specific batch of Cullinan Sand used for testing in this study were reported by Murison & Heymann (2024), and have been summarised in Table 1.

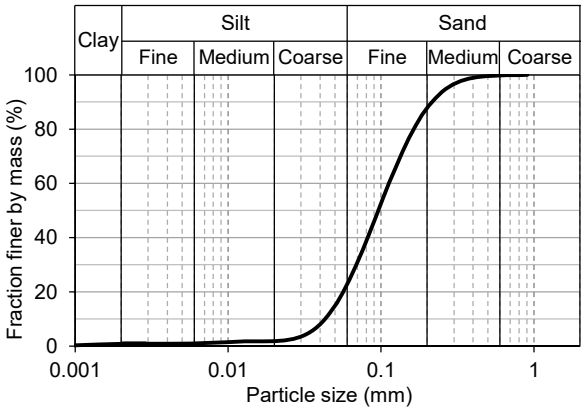

Figure 3. PSD of Cullinan Sand (after Murison & Heymann, 2024).

Table 1. Characteristic properties for Cullinan Sand (after Murison & Heymann, 2024).

Property	Value/description
USCS Classification	SPu
Mean particle size, d_{50} (mm)	0.096
[a] Fines content (<0.063 mm) (%)	23
[b] Fines content (<0.075 mm) (%)	33
Particle shape	Angular to subrounded
Specific gravity	2.694
Minimum dry density (kg/m^3)	1379
Maximum dry density (kg/m^3)	1704
Maximum void ratio, e_{max}	0.953
Minimum void ratio, e_{min}	0.576

[a] as defined in BS 1377 (1990)
[b] as defined in ASTM 2487 (2017)

4.2 *Testing programme*

One-dimensional compression tests were conducted using a GDS automatic oedometer (GDS Instruments, n.d.) that utilises a stationery load cell, with the position of the pedestal controlled using a stepper motor. The pedestal position was continuously automatically adjusted during the dissipation of the induced excess pore pressures in the sample, such that the user input target force was maintained as recorded by the load cell. Deformation of the sample during this process was recorded by a linear variable differential transformer (LVDT). Two-way vertical drainage was facilitated for all tests through top and bottom low air-entry porous ceramic discs, and the load cell force and LVDT displacement were logged at an interval of 1 second. The oedometer is depicted in Figure 4.

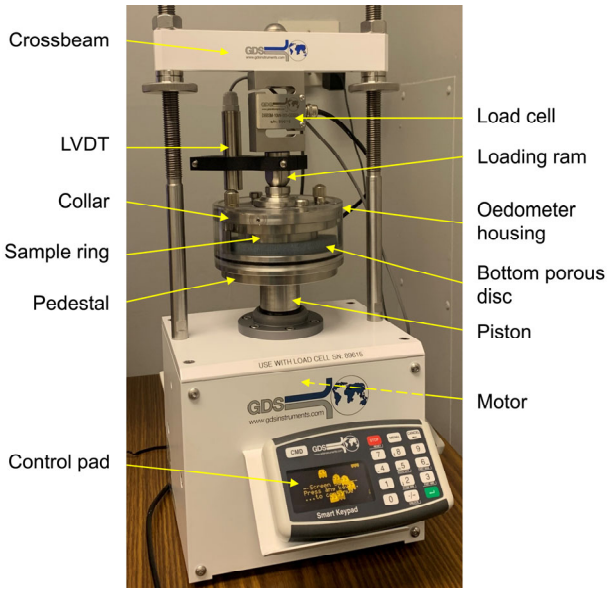

Figure 4. Automatic oedometer used in this study.

All tests were conducted in accordance with ASTM D2435 (2020) Method B. Samples were saturated under a nominal seating stress of 5 kPa, and time-deformation readings were recorded for the inundation phase and all subsequent loading and unloading increments. Although primary compression and swelling were complete within a matter of seconds for all increments in all tests, each increment was carried out for a minimum of 30 minutes. Samples were incrementally consolidated to a maximum vertical effective stress of 1500 kPa, after which unloading back to 5 kPa was conducted using half the number of increments applied during loading.

Three sample sizes were considered for this study. The average internal dimensions of the three oedometer rings are given in Table 2. The aspect ratio of each of the rings was within the limits specified by ASTM D2435 (2020), as discussed in Section 3. A visual representation of the varying sample diameter across the three sample sizes is given through the photograph of the Cullinan Sand oedometer specimens depicted in Figure 5.

Table 2. Average dimensions of oedometer rings used in this study.

Diameter, D (mm)	Height, H (mm)	Aspect ratio, H/D
50.02	20.01	0.400
70.07	19.02	0.271
75.06	19.10	0.254

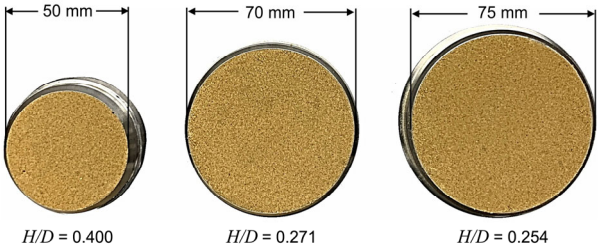

Figure 5. Visualisation of the sample sizes used in this study.

For each sample size, two oedometer tests were conducted. The two test sets were termed ‘loose’ and ‘medium dense’, and specific initial void ratios were targeted for each. The Cullinan Sand specimens were oven dried and mixed with water to achieve a target gravimetric water content of 8%. Samples were then remoulded and moist tamped into the oedometer rings, and the surface was levelled off with a spatula to ensure a known volume could be attained with bedding errors limited. Great care was taken with the initial sample masses such that the initial void ratios for each set were kept as constant as practically possible. The initial sample volume was assumed to be equal to the internal dimensions of the oedometer ring. For each test, the true mass of solids was determined after oven-drying the entire sample at 105°C for 24 h post-test, using a mass balance with a resolution of 0.001 g. The initial void ratios (e_0) achieved for each test are given in Table 3, along with the corresponding initial relative densities ($D_{r,0}$) calculated based on the index void ratios reported in Table 1.

Table 3. Initial conditions for each oedometer test.

Aspect ratio, H/D	‘Loose’ test	‘Medium dense’ test
0.400	$e_0 = 0.930$ $D_{r,0} = 6.0\%$	$e_0 = 0.785$ $D_{r,0} = 44.4\%$
0.271	$e_0 = 0.925$ $D_{r,0} = 7.4\%$	$e_0 = 0.788$ $D_{r,0} = 43.8\%$
0.254	$e_0 = 0.924$ $D_{r,0} = 7.6\%$	$e_0 = 0.780$ $D_{r,0} = 46.0\%$

5 RESULTS AND DISCUSSION

The compression curves and unloading curves are given for each of the loose and medium dense tests in Figure 6a and 6b respectively.

The initially loose samples could be tamped into the oedometer rings with minimal compaction effort and without imposing significant stress history upon the soil. These samples were thus considered to be normally consolidated from the outset of the test. Prior to inundation, each of the samples existed in a meta-stable state under the total stress of 5 kPa, due to the compaction-induced fabric as well as suctions in the initially unsaturated soil. Upon flooding the cell, wetting-induced collapse occurred for each of the loose samples, indicated by a void ratio reduction of between approximately 0.03 and 0.05 in Figure 6a. After inundation, each of the samples was loaded along what was considered to be the same measured one-dimensional normal consolidation line (1D NCL) for all practical purposes. The slopes of the swelling lines recorded during unloading were also reasonably similar.

Each of the samples in the medium dense test set required some mechanical compaction effort during preparation, and were thus initially overconsolidated. Minimal collapse upon inundation occurred for these samples (change in void ratio of between 0.004 to 0.007). Casagrande constructions (Casagrande, 1936) were carried out for each of the compression paths and indicated that the yield stresses ranged between 70 and 120 kPa, beyond which the samples were considered normally consolidated. Beyond yielding, the 50 mm diameter sample exhibited the stiffest response, followed by the 70 mm and 75 mm samples respectively.

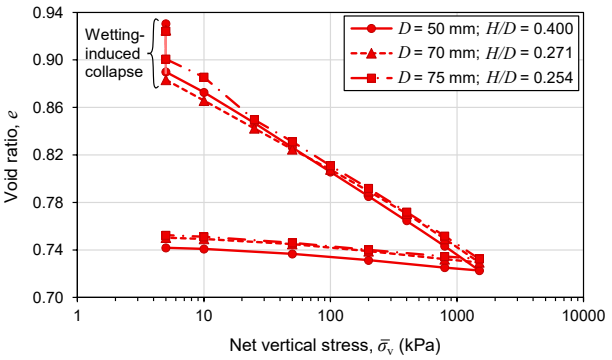

a) Loose tests, $e_0 \approx$ 0.92–0.93

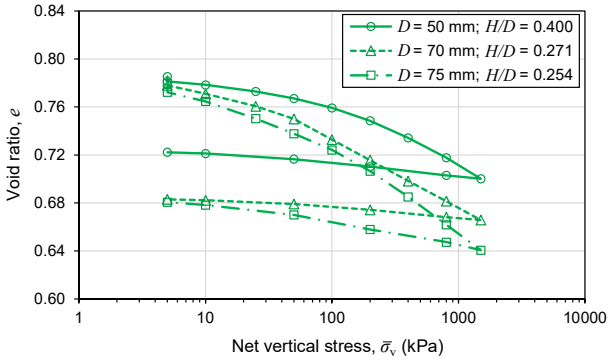

b) Medium dense tests, $e_0 \approx$ 0.78–0.79

Figure 6. Compression and unloading curves for each sample.

The variation of the slope of the one-dimensional NCL in semi-log space (compression index, C_c) across the varying relative density and sample size is shown in Figure 7. The compression indices were calculated over the 200 to 1500 kPa range for all samples to ensure that only normally consolidated behaviour was captured, and the expansion indices (C_e: slopes of swelling lines in semi-log space) were determined over the entire unloading range. Compression and expansion indices for each test are reported in Table 4. Figure 8 shows a summary of all the compression paths measured, relative to the theoretical minimum and maximum void ratios according to ASTM D4253 (2016) and D4254 (2016). Figures 7 and 8 show that the 1D NCL of the 75 mm medium dense sample was approximately parallel to the 1D NCLs measured for the loose samples. This observation aligns with the conceptual compression model outlined for sands in Figure 1, as proposed by Jefferies & Been (2000). The medium dense samples with smaller diameters exhibited lower compression indices. The expansion indices across all six samples remained relatively unchanged, perhaps with the exception of the 75 mm medium dense sample, which showed marginally greater recovery of elastic deformation during unloading.

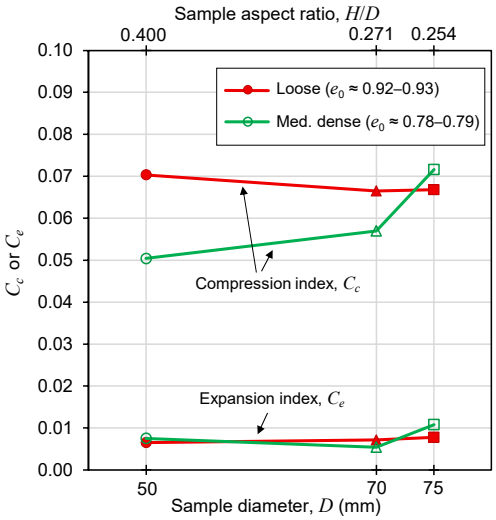

Figure 7. Compression and expansion indices versus aspect ratio.

Table 4. Compression and expansion indices.

Aspect ratio, H/D	'Loose' test	'Medium dense' test
0.400	$C_c = 0.0703$ $C_e = 0.0065$	$C_c = 0.0504$ $C_e = 0.0075$
0.271	$C_c = 0.0665$ $C_e = 0.0072$	$C_c = 0.0570$ $C_e = 0.0054$
0.254	$C_c = 0.0668$ $C_e = 0.0078$	$C_c = 0.0716$ $C_e = 0.0108$

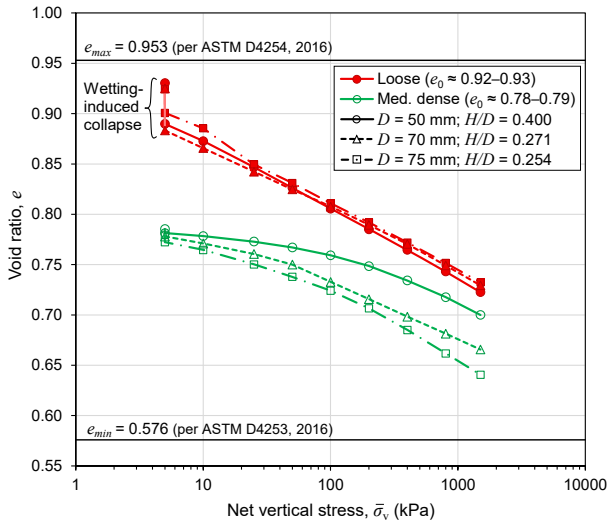

Figure 8. Summary of oedometer compression paths.

Considering a critical state soil mechanics framework, the three samples in a very loose state were likely wet-of-critical throughout loading, whereas the three denser samples were likely dry-of-critical even in their normally consolidated state. Dry-of-critical sands tend to exhibit a dilative response (i.e. tendency for volume increase) when sheared. It is proposed that the particles near the soil-ring interface along which shear stresses were mobilised were subjected to a dilative response as plastic strains were generated during virgin loading. This mechanism (which tends to cause volume increase) counteracts the compressive mechanism driving volume decrease due to the increasing vertical stress. For three samples at the same initial density, contained within sample rings made of the same material, the magnitudes of shear stresses and the extents of the zones of influence of the dilative mechanism were likely nearly identical. However, with a decreasing diameter (i.e. increasing H/D ratio) the impact of this mechanism upon the global compression behaviour would be greater, as the zone of influence takes up a greater proportion of the loaded area of the sample. Dilation is not a factor to be considered during the recovery of elastic strains during unloading, which supports the observation that the slopes of the swelling lines (C_e) were not significantly influenced by initial density or sample aspect ratio.

To provide justification for this proposed mechanism of dilation, the state throughout loading of each sample relative to the critical state line (CSL) was estimated. Crous and Jacobsz (2025) reported a unique CSL for Cullinan Sand, determined from a series of isotropically consolidated tests sheared both drained (CID) and undrained (CIU) in triaxial compression, from both loose and dense initial states. The parameters determined for the CSL are reported in Table 5. Mean effective stress (p') values for the anisotropically consolidated oedometer loading paths were estimated using Equation 2. The coefficient of earth pressure at rest (K_0) was assumed to remain constant for all values of vertical effective stress (σ'_v), and was estimated using the formulation by Jáky (1948) for normally consolidated uncemented soils ($K_0 = 1 - \sin\phi'_{cs}$).

$$p' = \frac{1}{3}[\sigma'_v(1 + 2K_0)] \quad (2)$$

Table 5. Critical state line for Cullinan Sand (after Crous and Jacobsz, 2025).

Parameter	Value
Critical void ratio at p' = 1 kPa, Γ	0.8698
Slope of CSL in e-ln p' space, λ_e	0.0202
Slope of CSL in e-log$_{10}$ p' space, λ_{10}	0.0465
Critical state friction ratio in triaxial compression, M_{tc}	1.329
Critical state friction angle, ϕ'_{cs} (°)	33.0

The estimated oedometer loading paths in mean effective stress space are plotted relative to the critical state line in Figure 9. It has been established in literature that as long as K_0 remains constant, anistropically consolidated loading paths are parallel to isotropic loading paths for normally consolidated soils (Coop, 1990; Atkinson and Bransby, 1978). Although only $K_0 = 0.455$ has been included in Figure 9, for any reasonable assumption of K_0, the loose tests plot above the CSL (i.e. in a wet-of-critical regime) for nearly the entire stress range, and the medium dense tests plot below the CSL (in a dry-of-critical regime) over the entire stress range. This implies that the sand near the soil–ring interface for the medium dense samples would indeed tend to dilate when subjected to shear stresses, and that that of the loose samples would not, the implication of which was previously discussed.

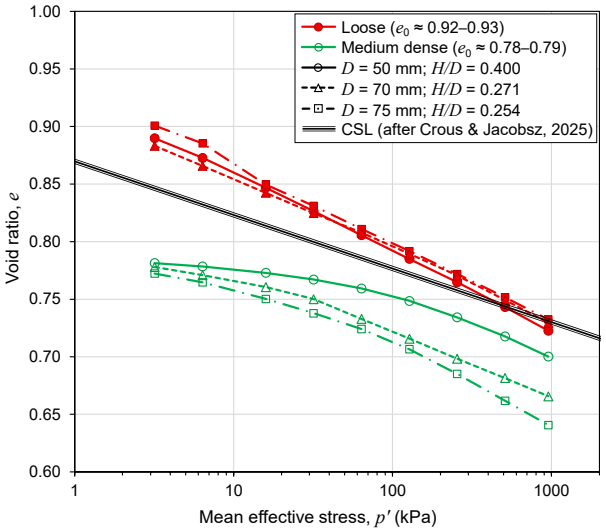

Figure 9. Oedometer test results assuming a constant K_0 from Jáky's (1948) equation, relative to the critical state line for Cullinan Sand determined by Crous & Jacobsz (2025).

Another explanation for the variation in compression paths of the medium dense samples is the presence of greater initial horizontal stresses in the denser soil, which was subjected to greater compaction energy prior to testing. Per Figure 2, greater horizontal stress would cause a greater resultant force acting on the side wall and greater shear stresses mobilised along the interface. Equation 1 shows that this would lead to a greater variation in vertical effective stress within the sample and greater deviations from true one-dimensional compression when compared to the loose samples. For the same reasons mentioned previously and with reference to Equation 1, the influence of this error would reduce with increasing sample diameter (i.e. decreasing H/D).

Based on these results, it is clear that the recommended minimum aspect ratio of $H/D = 0.4$ (ASTM D2435, 2020) is not sufficient to avoid errors in measured compressibility of dry-of-critical sand samples. In the present study, an aspect ratio of $H/D = 0.254$ was sufficiently small to negate the effects of side wall friction. In general, the H/D ratio beyond which the error becomes significant is likely soil type and density dependent. It is thus preliminarily recommended that H/D should be minimised as far as practically possible for oedometer testing of coarse-grained soils.

6 CONCLUSIONS

The influence of oedometer sample aspect ratio was investigated for both loose and medium dense samples of a remoulded uncemented silica sand. The tests on initially loose samples (relative density of ~ 6-8%) showed no significant influence of sample aspect ratio on the measured one-dimensional normal consolidation line. For the initially medium dense samples (relative density of ~ 44-46%), the measured compression index (C_c) reduced with increasing height-to-diameter aspect ratios. This reduction in compressibility was attributed to the dilative tendency of sand subjected to shear stresses at the ring interface. When the height-to-diameter ratio of a dry-of-critical sand sample is not sufficiently minimised, the influence of this dilation (which counteracts compression of the sample) becomes significant. The initially medium dense sample with the lowest height-to-diameter aspect ratio was loaded along a normal consolidation line that was

approximately parallel to the compression paths of the loose tests, which agrees with the framework proposed by Jefferies & Been (2000). Expansion indices (C_e) were not significantly influenced by initial density nor sample aspect ratio. The unloading lines for all samples were approximately parallel, once again conforming with the theoretical compression framework outlined for sands. Although an aspect ratio of $H/D = 0.254$ was considered satisfactorily small to negate the effects of dilation due to side wall friction in this study, the required aspect ratio would be dependent on the soil and density being considered. It is thus recommended that the H/D ratio be minimised as far as practically possible to avoid errors in measured compression behaviour whenever dense coarse-grained soils are being tested in the oedometer.

7 ACKNOWLEDGEMENTS

The first author gratefully acknowledges the Geotechnical Division of the South African Institution of Civil Engineering (SAICE GeoDiv) for sponsoring his conference attendance.

8 REFERENCES

ASTM. 2014. *D5550-14: Standard Test Method for Specific Gravity of Soil Solids by Gas Pycnometer.* West Conshohocken: ASTM International.

ASTM. 2016. *D4253-16: Standard Test Methods for Maximum Index Density and Unit Weight of Soils Using a Vibratory Table*. West Conshohocken: ASTM International.

ASTM. 2016. *D4254-16: Standard Test Methods for Minimum Index Density and Unit Weight of Soils and Calculation of Relative Density*. West Conshohocken: ASTM International.

ASTM. 2017. *ASTM D2487-17: Standard Practice for Classification of Soils for Engineering Purposes (Unified Soil Classification System)*. West Conshohocken: ASTM International.

ASTM. 2020. *D2435-20: Standard Test Methods for One-Dimensional Consolidation Properties of Soils Using Incremental Loading*. West Conshohocken: ASTM International.

Atkinson, J.H. and Bransby, P.L. 1978. *The mechanics of soils: an introduction to critical state soil mechanics*. London: McGraw Hill.

BSI. 1990. *BS 1377-2:1990. Methods of test for soils for civil engineering purposes – Part 2: Classification tests*. London: British Standards Institution.

Burland, J.B. 1990. On the compressibility and shear strength of natural clays (30th Rankine Lecture). *Géotechnique* 40(3), 329-378.

Casagrande, A. 1936. The determination of the pre-consolidation load and its practical significance. *Proc.: 1st International Conference on Soil Mechanics and Foundation Engineering, Harvard, May 1936*, 3, 60-64. London: ISSMFE.

Coop, M.R. 1990. The mechanics of uncemented carbonate sands. *Géotechnique* 40(4), 607-626.

Crous, P.A. and Jacobsz, S.W. 2025. Capabilities and constraints of NorSand in modelling slope instability. *Proc.: 2nd Southern African Geotechnical Conference, uMhlanga, May 2025*.

GDS Instruments. n.d. *Automatic Oedometer System (GDSAOS) (One Dimensional Consolidation) – Datasheet.*

Henkel, D.J. 1960. The relationships between the effective stresses and water content in saturated clays. *Géotechnique* 10(2),41-54.

International Organization for Standardization. 2020. *ISO 13320: Particle size analysis - Laser diffraction methods*. Geneva: ISO.

Ishihara, K., Tatsuoka, F. and Yasuda, S. 1975. Undrained deformation and liquefaction of sand under cyclic stresses. *Soils and Foundations* 15(1), 29-44.

Jáky, J. 1948. Pressure in silos. *Proc.: 2nd International Conference on Soil Mechanics and Foundation Engineering, Rotterdam, June 1948*, 1, 103-107. Haarlem: Gebr. Keesmaat

Jefferies, M.G. and Been, K. 2000. Implications for critical state theory from isotropic compression of sand. *Géotechnique* 50(4), 419-429.

Leroueil, S. and Vaughan, P.R. 1990. The general and congruent effects of structure in natural soils and weak rocks. *Géotechnique* 40(3), 467-488.

Murison, R.A. and Heymann, G. 2024. Using shear modulus to predict the bearing capacity of strip foundations on sand. *E3S Web of Conferences* 544, 07005.

Narainsamy, Y., Jacobsz, S.W., Murison, R.A. and Vermeulen, N.J. 2023. Uniqueness of the normal consolidation line for gold tailings. *Geotechnical Testing Journal* 46(6), 1046-1054.

Pestana, J.M. and Whittle, A.J. 1995. Compression model for cohesionless soils. *Géotechnique* 45(4), 611-631.

Rendulic, L. 1937. Ein Grundgesetz der Tonmechanik und sein experimenteller Beweis. *Der Bauingenieur* 18(31), 459-467.

Roscoe, K.H. and Burland, J.B. 1968. On the generalised stress-strain behaviour of 'wet' clays. In *Engineering Plasticity: Papers for a Conference Held in Cambridge, March 1968, ed. J. Heyman and F.A. Leckie*, 535–609. Cambridge: Cambridge University Press.

Schofield, A.N. and Wroth, C.P. 1968. *Critical state soil mechanics*. London: McGraw-Hill.

Skempton, A.W. 1944. Notes on the compressibility of clays. *Quarterly Journal of the Geological Society* 100(2), 119-135.

Terzaghi, K. von. 1923. Die Berechnung der Durchlässigkeitsziffer des Tones aus dem Verlauf der hydrodynamischen Spannungserscheinungen. *Sitzungsbrichte der Akademie der Wissenschaften in Wien Mathematisch-Naturwissenschaftliche Klasse* 132(Iia), 125-138.

Terzaghi, K. von. 1925. *Erdbaumechanik auf Bodenphysikalischer Grundlage*. Wien: Frans Deuticke.